

Automated Scoring of Nuclear Pleomorphism Spectrum with Pathologist-level Performance in Breast Cancer

Caner Mercan^{a,*}, Maschenka Balkenhol^a, Roberto Salgado^{b,c}, Mark Sherman^d, Philippe Vielh^e, Willem Vreuls^f, António Polónia^g, Hugo M. Horlings^h, Wilko Weichertⁱ, Jodi M. Carter^d, Peter Bult^a, Matthias Christgen^j, Carsten Denkert^k, Koen van de Vijver^l, Jeroen van der Laak^a, and Francesco Ciompi^a

^aRadboud University Medical Center, Radboud Institute for Health Sciences, Department of Pathology, Nijmegen, The Netherlands

^bGZA-ZNA Hospitals, Department of Pathology, Antwerp, Belgium

^cPeter Mac Callum Cancer Centre, Division of Research, Melbourne, Australia

^dMayo Clinic, Department of Laboratory Medicine and Pathology, Rochester, Minnesota, USA

^eMedipath & American Hospital of Paris, Paris, France

^fCanisius Wilhelmina Ziekenhuis, Nijmegen, The Netherlands

^gUniversity of Porto, Institute of Molecular Pathology and Immunology Department of Pathology, Ipatimup Diagnostics, Porto, Portugal

^hThe Netherlands Cancer Institute, Department of Molecular Pathology, Amsterdam, The Netherlands

ⁱTechnical University Munich, Institute of Pathology, Munich, Germany

^jHannover Medical School, Institute of Pathology, Hannover, Germany

^kPhilipps University of Marburg, Institute of Pathology, Marburg, Germany

^lGhent University Hospital and Cancer Research Institute Ghent, Department of Pathology, Ghent, Belgium

*e-mail: caner.mercan@radboudumc.nl

ABSTRACT

Nuclear pleomorphism is the degree of change in nuclear morphology, one of the components of the three-tiered breast cancer grading, along with tubular differentiation and mitotic counting. The degree of nuclear pleomorphism is reflected in a three-category classification of tumor where a score of 1 resembles normal breast epithelium, a score of 2 corresponds to moderate morphological changes and a score of 3 is assigned for highly pleomorphic nuclei. In contrast to the other two quantitative components in breast cancer grading, establishing a reference standard is very difficult as the qualitative assessment of the degree of nuclear pleomorphism has to be converted in a score. As a result, scoring nuclear pleomorphism suffers from a low agreement between pathologists. In this paper, we consider the degree of nuclear pleomorphism as a continuum; a continuous spectrum of change in tumor morphology. We train a deep learning network on a large variety of tumor regions from the collective knowledge of several pathologists without constraining the network to the traditional three-category classification. We also motivate an additional approach in which we discuss the additional benefit of normal epithelium as baseline, following the routine clinical practice where pathologists are trained to score nuclear pleomorphism in tumor, having the normal breast epithelium as baseline. In multiple experiments, our fully-automated approach could achieve top pathologist-level performance in select regions of interest as well as at whole slide images, compared to ten and four pathologists, respectively.

1 Introduction

In 2020, breast cancer remains the most prevalent cancer in women, and is second in mortality rate behind lung cancer in the United States [34]. Every newly diagnosed breast cancer will undergo histological grading by means of the modified Bloom and Richardson grading system [7, 12]. It is comprised of three components to assess the degree of differentiation of the invasive tumor in breast tissues. The scoring criteria for mitotic counting and tubular differentiation are defined by quantitative measures whereas nuclear pleomorphism scoring is based on qualitative analysis of the nuclear morphology of tumor. The score of tumor pleomorphism is 1 if the size, shape and the structure of the cells resemble normal breast epithelium. It is a score of 2, if the nuclear morphology changes moderately, the cells have open vesicular nuclei with visible nucleoli. The score of pleomorphism is 3 when the tumor morphology is aberrant, cells having vesicular nuclei with prominent nucleoli. This process is traditionally performed through microscopical examination of breast cancer tissue sections by pathologists. With the surge of

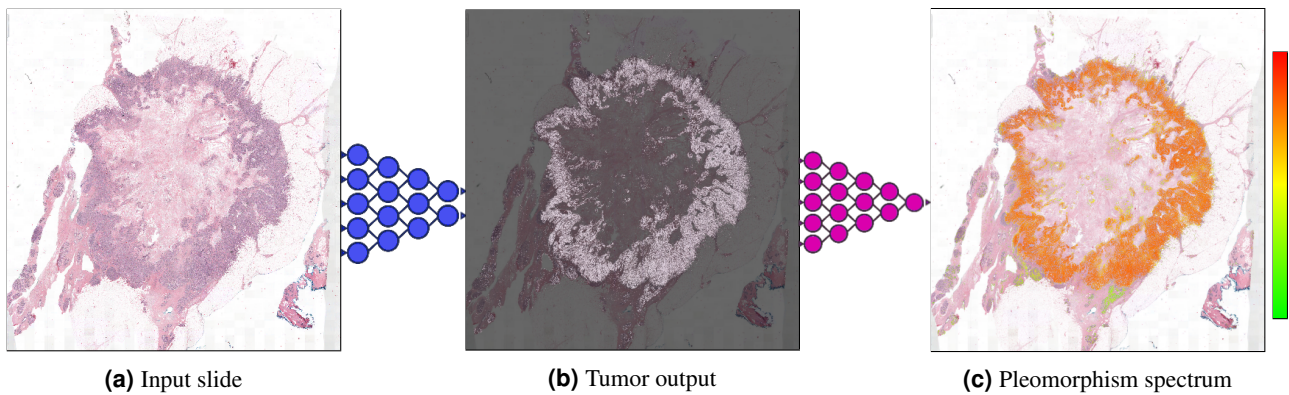


Figure 1. The overview of the AI algorithm scoring nuclear pleomorphism spectrum. An input whole slide image (a) is processed through the epithelial cell detection network to detect the tumor regions. Subsequently, the deep regression network scores nuclear pleomorphism on the tumor regions, score 1 is denoted by green, score 2 by yellow and score 3 by red color. Since the deep regression network outputs a spectrum of values, ranging from 1 to 3, reflecting the scores in between the traditional three categories, as well. In this example, the AI algorithm scored high pleomorphism for the tumor regions in the input slide, evident by the dark orange and red colors in the pleomorphism spectrum.

digital pathology, these tasks can now be carried out on digitized histopathological images without any decline in concordance among pathologists as compared to assessment via light microscopy [15]. Also, the pathologists can be assisted by Artificial Intelligence (AI) based systems in routine practice [6, 30, 8, 2].

Deep learning architectures are composed of connected neurons that receive an input image and perform a series of operations on the learnable network weights to accomplish a learning task, such as classification, regression and segmentation. The field of AI has seen unprecedented success in several areas of computer vision [18, 19, 35, 11] to more recent advancements in digital pathology [1, 5, 39, 28, 9] with the bloom of deep learning. More specific for breast cancer grading, automated mitosis detection was one of the first digital pathology applications using deep learning [10, 38], demonstrating the clinical and prognostic value of automated mitotic counting [37, 3, 4]. Tubule segmentation was formulated as a series of nuclei and gland detection, as well as a segmentation task [29, 20], with extensions to clinical risk categories [32] through the use of deep learning. Unlike tubular differentiation and mitotic counting, nuclear pleomorphism does not have the same quantitative nature in its definition. As a result, the degree of pathologist disagreement in nuclear pleomorphism has a long history of being the worst of the three grading criteria [13, 27, 22]. On top of that, the works addressing automated nuclear pleomorphism scoring have been limited, consisting of techniques involving manually crafted nuclear features [23, 14] combined with the use of deep belief networks [24], descriptor based pixel-level image features [17] or binary classification of high pleomorphism (score 3) vs. not using a simple convolutional neural network on small image patches [31].

In this work, we formulate a novel AI-based approach to nuclear pleomorphism scoring by considering it as a continuum, a full spectrum of the change in tumor morphology, rather than classifying it into three discrete categories. We achieve this by re-formulating the original three-category classification into a full spectrum of continuous values from the lowest pleomorphism score to most severe. Our approach mainly consisted of two parts. The first part was the automated tumor region detection by our epithelial cell detection network from a previous work [26]. This step ensured that only the diagnostically relevant regions (i.e. invasive tumor) would be processed in an input whole slide image. In the second part, our deep regression network predicted nuclear pleomorphism spectrum on the tumor regions. This work marks the first end-to-end fully automated nuclear pleomorphism scoring in breast cancer using deep learning. The overview of the AI algorithm outlining this two-stage process of nuclear pleomorphism scoring is presented in Figure 1.

In order to achieve and validate our approach, we carried out two separate studies, resulting in two separate data sets. The first study, referred to as ROI-study, consisted of 125 tumor regions of interest (tumor ROIs) and an additional 79 healthy epithelial regions of interest (normal ROIs) from 39 whole slide images, carefully selected to include a wide variety of tumor morphology in breast cancer histopathology. We invited 10 pathologists from 6 countries to score nuclear pleomorphism on the tumor ROIs, each paired with a normal ROI visually for the pathologists to use as reference for scoring pleomorphism. We used the ROI-study to train our AI algorithm as well as to evaluate its performance compared to the panel of pathologists. In our automated approach, the reference scores were the collective knowledge computed from the averaged nuclear pleomorphism scores of the pathologists. The AI algorithm was trained on a wide range of tumor morphology, leveraging the reference scores to establish the concept of nuclear pleomorphism as a full spectrum of tumor morphology change. In the second study, referred to as slide-study, 118 whole slide images were selected for the evaluation of the trained AI algorithm. The distribution of the

	<i>MAE</i> ↓	<i>MSE</i> ↓	<i>MdAE</i> ↓	<i>EV</i> ↑	<i>R</i> ² ↑
AI algorithm	0.262 ± 0.004	0.111 ± 0.002	0.215 ± 0.008	0.758 ± 0.008	0.756 ± 0.009
AI algorithm with baseline	0.275 ± 0.006	0.116 ± 0.007	0.237 ± 0.014	0.744 ± 0.014	0.743 ± 0.016

Table 1. Evaluation of the added value of normal epithelium as a baseline on a subset of the patches in the validation set of the ROI-study. AI algorithm refers to learning from tumor morphology whereas AI algorithm with baseline refers to the extension in which normal epithelium is used as baseline. Performance is better when mean absolute error (*MAE*), mean squared error (*MSE*) and median absolute error (*MdAE*) are low, explained variance score (*EV*) and *R*² score are high.

slides resembled the distribution of the cases in routine clinical practice. For the slide-study, we invited 4 pathologists to score nuclear pleomorphism of the slides which were compared to our AI algorithm for whole slide-level evaluation. More details on the ROI-study and slide-study are provided in Section 4.

2 Results

Is tumor morphology enough for automated nuclear pleomorphism scoring? In routine clinical practice, pathologists score nuclear pleomorphism of tumor via a visual comparison to a region with normal cells as reference. In this section, we discuss whether the tumor morphology by itself is enough for the AI algorithm to learn the full pleomorphism spectrum without having seen any examples from healthy epithelium. Therefore, we investigated two approaches, one consisting of learning only from tumor morphology and another one incorporating normal epithelium on top of the first approach. The former was an AI algorithm trained and validated only on tumor patches from the training and validation sets in the ROI-study. For the second approach, we also incorporated the normal ROIs to sample patches with normal cells (see Section 4 for details). We compared the best models from both approaches on four independent sets of 1000 patches randomly sampled from the validation set. For each input patch, the predictions from both models were nuclear pleomorphism scores of continuous values between $[1 - \epsilon, 3 + \epsilon]$. We evaluated both models on several regression metrics in comparison to the reference scores, as presented in Table 1. The results highlighted that the AI algorithm could learn the nuclear pleomorphism spectrum well enough from the tumor morphology alone. The AI algorithm was trained on such a wide variety of tumor morphology (see Figure 8) that it did not need normal epithelium as a baseline. In the rest of the paper, we report the results from the AI algorithm that was trained only on tumor morphology.

Prediction performance of the AI algorithm on patches. In this section, we analyze the predictions of the AI algorithm on fixed-sized patches of 512×512 pixels randomly cropped at $20\times$ magnification from 45 ROIs out of the 13 test slides in our ROI data set. The output of our AI algorithm is a continuous numerical value ranging between $1 - \epsilon$ to $3 + \epsilon$, corresponding to the increasing severity of the nuclear pleomorphism. In order to demonstrate the granularity of our automated approach, we quantized the AI algorithm predictions into three (similar to the routine practice as per the guidelines), as well as five and nine categories. In Figure 2, we present several patches from the test set for each category. In every category, the patches were sorted by the quantized predictions of the AI algorithm, with each patch having a higher categorical predicted score than the one preceding it. As the pleomorphism predictions went from low to high, the tumor morphology became more aberrant at each step. While the nuclei in the leftmost patches resembled the most to healthy epithelium in appearance, the nuclear pleomorphism became gradually more severe with each patch to the right.

Making correct predictions is important, but what is more important is making correct predictions with correct reasoning. To investigate this, we resort to an approach called Gradient-weighted Class Activation Mapping (Grad-CAM) [33]. The main idea behind Grad-CAM is to highlight the areas in an input image patch that played a role in the prediction output of that patch. We employed this idea on our deep regression network to see whether the predictions were made by taking the nuclear morphology into account. In Figure 3, we present several example patches from the test set in our ROI data set, visualizing the salient areas determined by the deep regression network. The patches with predictions close to the reference scores showed strong activation around nuclei. Similarly, when we inspected the patches where the AI algorithm failed, we observed that it overlooked the nuclear structures, reflected by the salient areas on other tissue parts. Our experiments in this section indicated that the AI algorithm predicted similar scores with the pathologists when it focused on the nuclei, failing when focusing on other areas, such as stroma. We overcame this problem by processing multiple overlapping patches from the same area with small displacements. This ensured that the AI algorithm saw a slightly displaced patch and it mostly focused on the same nuclear areas. As a result, the predictions were, on average, based on the nuclear architectures, as the problem occurred few and far between.

Quantitative evaluation of the AI algorithm vs. pathologists. For the first quantitative analysis of the AI algorithm compared to pathologists, we considered a controlled test scenario on the evaluation set of the ROI-study. This ensured that

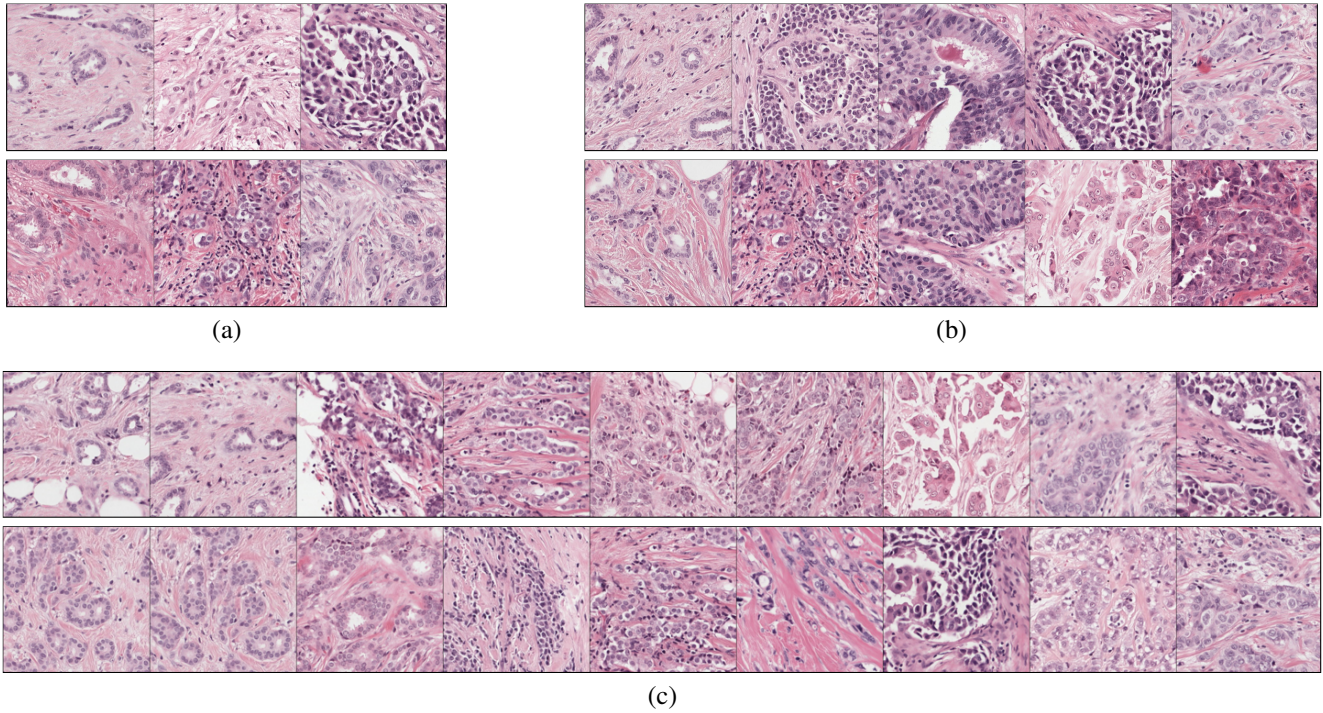


Figure 2. Nuclear pleomorphism predictions quantized into different number of categories, sorted from low pleomorphism to high in each category, from left to right. In (a), patches are quantized into three categories which is in line with the traditional three-category classification, whereas in (b) and (c), the patches are quantized into five and nine categories, respectively, to demonstrate the continuity of the nuclear pleomorphism spectrum from the predictions of the AI algorithm.

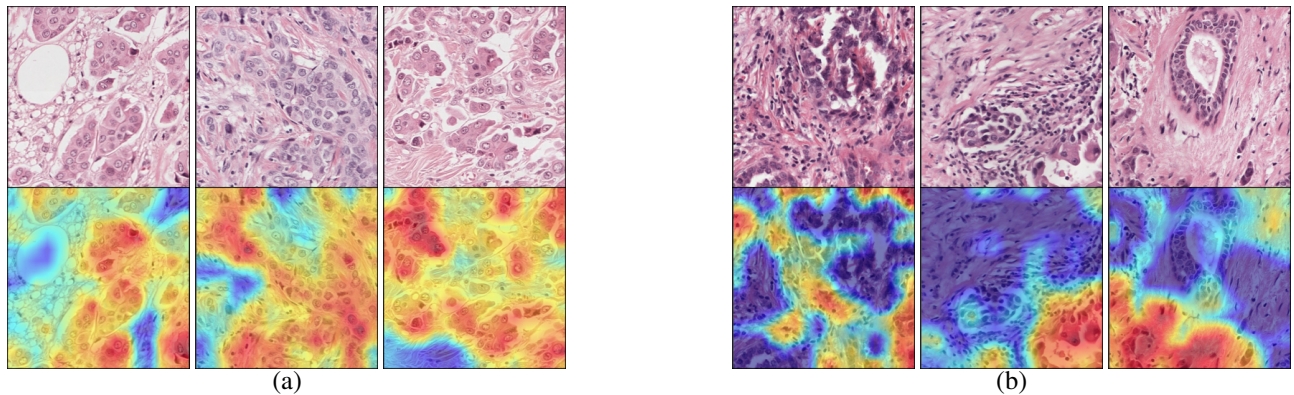


Figure 3. Grad-CAM saliency outputs of six patches from the evaluation set in the ROI-study. The predictions were close to the reference scores when the AI algorithm focused on the cellular structures (a), and it failed in few cases focusing on other tissue parts (b).

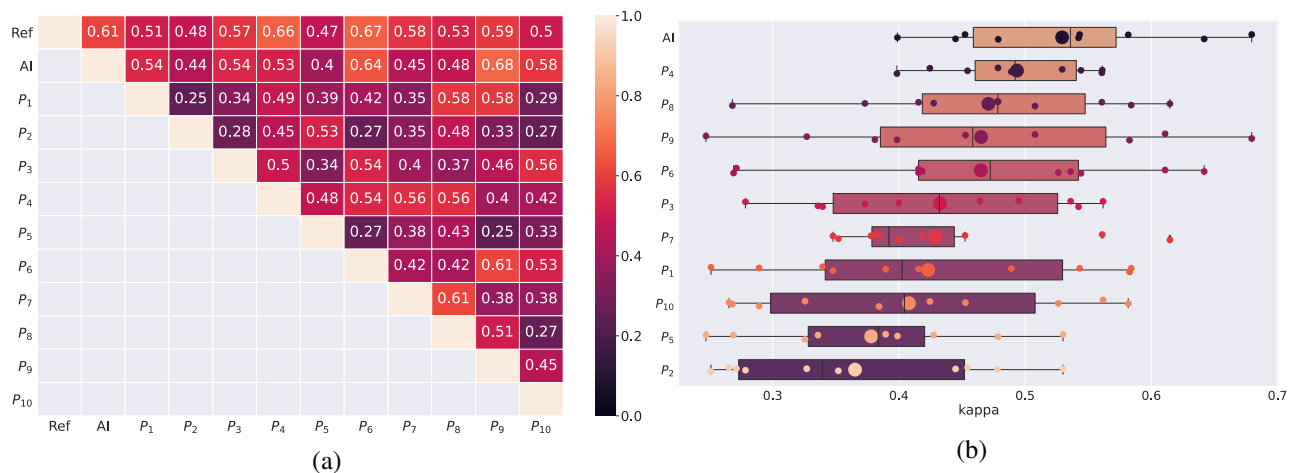


Figure 4. The quadratic kappa scores of the pathologists as well as the AI algorithm on the evaluation set in the ROI-study (45 ROIs). In (a), pairwise kappa scores of the AI algorithm and the pathologists are compared where the best pairwise kappa score was achieved between the AI algorithm and P₉. The majority scores, denoted by Ref, had the third best kappa score with the AI algorithm, behind P₆ and P₄. The pairwise kappa metrics, sorted by the average pairwise scores, (b) shows that the AI algorithm has, on average, the highest agreement out of any pathologists. It also has the highest pairwise kappa score of 0.68 with P₉. In each row, small dots corresponds to the kappa scores with the other pathologists/AI algorithm and the large dot denotes the average kappa score of that particular pathologist/AI algorithm with the others.

an ROI contained the same degree of pleomorphism in its tumor cells. This evaluation set consisted of 45 ROIs from 13 slides. Each pathologist scored nuclear pleomorphism on these tumor ROIs into one of the three categories, $\{1, 2, 3\}$. As the input to the AI algorithm was of size 512×512 pixels, the ROIs were too large to be processed directly. Therefore, a single pleomorphism score for an ROI was obtained by the procedure below. The ROI was processed into fixed-size overlapping tiles. In our experiments, we utilized an overlap value of 448 pixels, horizontally and vertically, for the tile size of 512×512 pixels. The AI algorithm predicted a continuous pleomorphism score for each tile. As a result of the overlapping tiles, multiple predictions were made in small blocks of size 64×64 and for each block in the ROI, predictions were aggregated by average pooling to assign its pleomorphism score. Subsequently, we fine-tuned the predictions by only assigning them to the tumor cells using the epithelial cell detection network. Finally, the pleomorphism score of the ROI was determined by the average pleomorphism score in the tumor. We quantized the predicted pleomorphism scores of ROIs into the traditional three categories to compare to the scores of the pathologists. The quantized predictions were also compared to the majority scores of the pathologists which were computed by taking the majority vote of their scores and the provided confidence scores in the case of ties. We present the kappa scores detailing the agreement comparisons of the pathologists and the AI algorithm in Figure 4. In this comparison, the scores of a pathologist were not included in the majority voting when that pathologist was compared to the majority scores. On the other hand, the scores of all pathologists were used for the majority voting for the comparison between the AI algorithm and the majority scores. The AI algorithm had a kappa score 0.61 with the majority scores, trailing behind only two pathologists, P₆ and P₄ with kappa scores 0.67 and 0.66 with the majority scores, respectively. Additionally, the AI algorithm had the highest average kappa score of 0.53, followed by the kappa score of 0.49 by P₄. The AI algorithm on average, showed the highest agreement, and it ranked third behind the two best performing pathologists when compared to the majority scores on the evaluation set in the ROI-study.

Real case application by scoring nuclear pleomorphism on whole slide images. This slide-level experimental setup was in-line with the real-world clinical setting, where an entire slide is assigned a single nuclear pleomorphism score by a pathologist. Here, we used the 118 whole slide images for the slide-level evaluation of the AI algorithm compared to the four participating pathologists, denoted by P_i, P_{ii}, P_{iii}, P_{iv}, who scored nuclear pleomorphism on the same set of slides into one of the three categories. It has to be noted that three of the four pathologists also participated in the ROI-level study, and one pathologist, P_{iv}, only participated in this slide level study. In contrast to the ROI-level study in which ROIs were selected to have homogeneous pleomorphism, tumor in whole slide images contained larger heterogeneity with more diverse nuclei morphology. The AI algorithm predictions for an input whole slide image followed a similar procedure with the ROI-level study. An additional preprocessing step was applied to locate and process only the tumor regions in the slide, using the output of the epithelial cell detection network to avoid fat, stroma, normal epithelium and several other structures that are not taken into account in breast cancer grading. Therefore, we ensured that the deep regression network scored pleomorphism only on

tumor regions. Finally, the pleomorphism score of the slide was determined by average pooling the pleomorphism spectrum of its tumor regions. We present the visual pleomorphism spectrum of the (non-quantized) predictions of the AI algorithm on four example slides from the slide-study in Figure 5.

For the quantitative analysis of the AI algorithm compared to the other pathologists over the 118 whole slide images, we quantized the pleomorphism predictions of the slides into one of the three categories. Figures 6a - 6d present the score difference of the AI algorithm compared to the pathologists. The AI algorithm scored the same nuclear pleomorphism score in 74, 66, 71 and 75 slides with pathologists $P_i, P_{ii}, P_{iii}, P_{iv}$, respectively. The AI algorithm had a score difference of ± 1 on the rest of the slides, except for the two slides in comparison to P_{ii} and one slide to P_{iv} where the pathologists scored 3 for the slides whereas the AI algorithm scored 1. For these slides, the scores of the other pathologists were (1, 2, 1), (2, 2, 2) and (2, 2, 2). Additionally, compared to the score differences of the pathologists, as seen in Figure 10, the AI algorithm had the most matching scores in 75 slides with P_{iv} as well as the highest matching scores, on average. Looking at the score distribution of the AI algorithm, we observe that the AI algorithm predicted the score 1 in 37 slides, score 2 in 70 slides and score 3 in 11 slides, as shown in Figure 6e. Finally, we present the kappa scores of the AI algorithm as well as the individual pathologists in Figure 6f. The highest kappa score of 0.56 was achieved between the AI algorithm and P_i . The AI algorithm had kappa scores of 0.43, 0.44 and 0.47 with the rest of the pathologists, P_{ii}, P_{iii}, P_{iv} , respectively. Overall, the average kappa score for the AI algorithm was 0.475 and it was only second to P_i with 0.497. P_i was also the participant with the overall highest average agreement. The results indicate that P_i agreed the most with the AI algorithm, more so than any other pathologists. Our findings in this slide-level study were consistent with our results in the previous experiments with the AI algorithm consistently ranking high in agreement with the best performing pathologists. Additionally, qualitative analysis of the predictions on whole slide images demonstrated that the AI algorithm learned to score the full spectrum of nuclear pleomorphism based on morphological changes in tumor cells.

3 Discussion

In this paper, we proposed a novel methodology for automated scoring of nuclear pleomorphism as a continuum in breast cancer. Our AI algorithm was composed of two stages. In the first stage, the epithelial cell detection network was used to locate tumor cells in whole slide images. In the second stage, the deep regression network scored nuclear pleomorphism on the tumor, considering the tumor pleomorphism as a spectrum. Our results showed that the AI algorithm consistently achieved top-level performance similar to the best performing pathologists throughout our experiments in ROI and slide-level studies.

In our experiments, we quantized the patch-level predictions of the AI algorithm into arbitrary number of categories to showcase its flexibility of demonstrating the continuity of the pleomorphism in tumor in greater granularity than the traditional three-category classification. In the few cases, the predictions failed to capture the pleomorphism in tumor when the AI algorithm did not focus on areas with tumor cells. We discovered that this shortcoming could easily be bypassed by processing multiple overlapping patches from the same area and average pooling the predictions, as the occurrence of the problem was few and far between. We also investigated the added value of normal epithelium as baseline, following the workflow of the pathologists in routine practice. The normal ROIs were less diverse compared to tumor ROIs, due to the slides containing only a handful very small areas with normal cells. In addition, due to the nature of normal epithelium, normal ROIs contained, on average, a larger ratio of stroma and ductal structures to cells. Therefore, we do not rule out the possibility that the AI algorithm might have focused on such structures more and failed to capture the nuclear morphology of normal cells. We leave the further investigation of this learning setup for future work. However, we proved that our automated approach could already learn the entire spectrum of tumor pleomorphism without additional knowledge of the normal cell morphology through multiple experiments.

In the ROI-study, the AI algorithm outperformed all 10 pathologists, achieving the highest overall pairwise kappa score as well as the highest average kappa score. This is an important outcome as it suggests that our approach is the best out of the participating pathologists at scoring pleomorphism on homogeneous tumor regions. The results of our experiments in the slide-study suggested a similar outcome with the AI algorithm achieving the second best average kappa score among four pathologists. In addition, the best performing pathologist with the highest average kappa score agreed the most with the AI algorithm by a large margin. In very few cases, where the epithelial cell detection network captured the tumor in regions with Ductal Carcinoma in Situ (DCIS), the deep regression network scored pleomorphism on those regions, too. We argue that the performance of the AI algorithm was slightly hampered by such false predictions causing the overall score of the slides to be quantized one score lower than the predictions of the deep regression network for the tumor actually suggested. This is also visible in the Figure 6e, as the predictions of the AI algorithm, on average, were slightly lower than that of the pathologists, as presented in Figure 8. This subsidiary issue could be mitigated by enriching the training set of the epithelial cell detection network with more examples from DCIS cases.

In this work, we proposed a fully automated deep learning methodology for the generalized version of the traditional three-category classification of nuclear pleomorphism in breast cancer, formulated as a continuous spectrum of the entire tumor

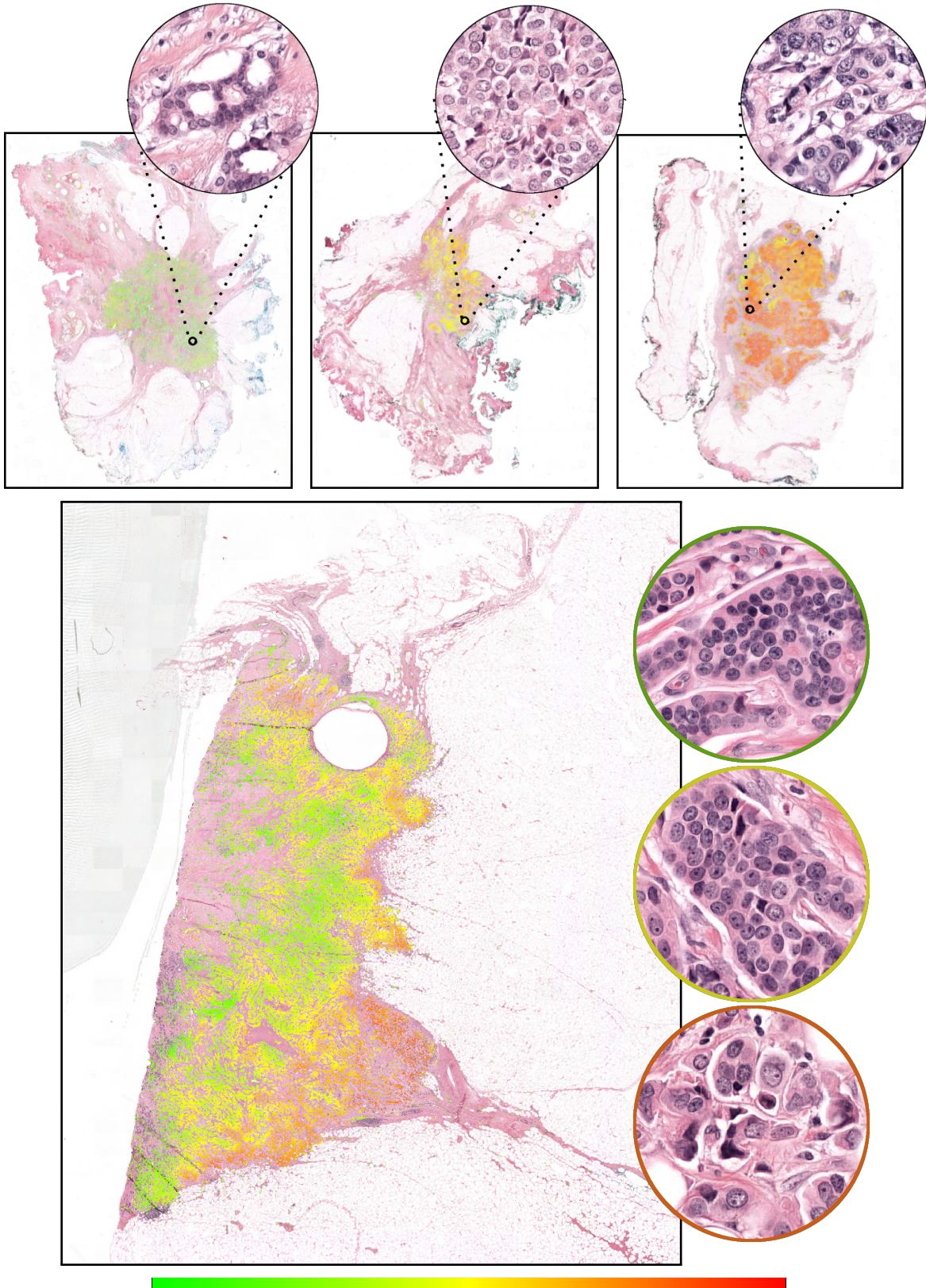


Figure 5. Nuclear pleomorphism spectrum of the AI algorithm on four of the 118 test slides. The color spectrum from green to yellow to red denotes increasing nuclear pleomorphism severity. The deformation in nuclear morphology with the increasing pleomorphism scores demonstrates the capability of the AI algorithm capturing the concept of nuclear pleomorphism.

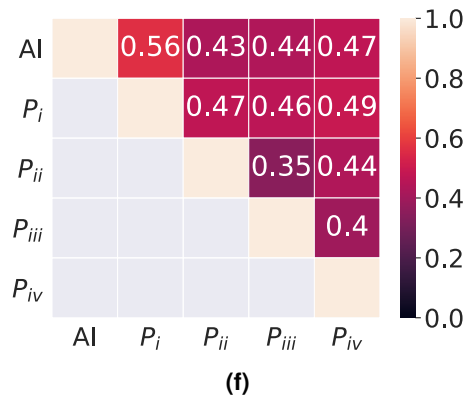
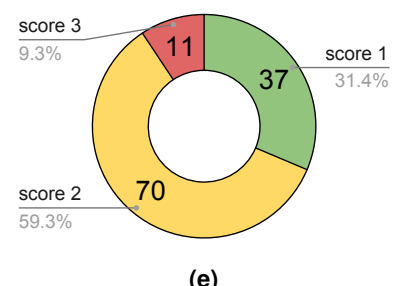
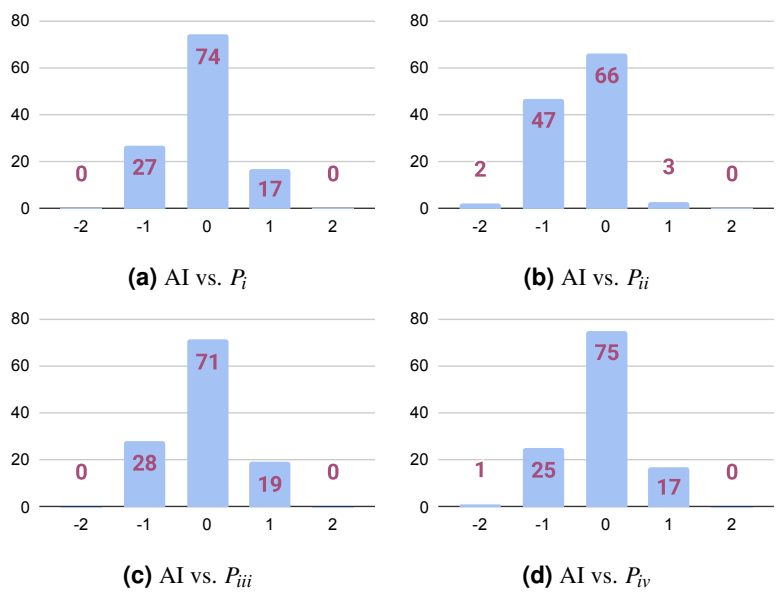


Figure 6. The evaluation of the performance of the AI algorithm on 118 evaluation slides in the slide-study. The scores of the AI algorithm are quantized into three categories. The differences in scores of the AI algorithm from the scores given by the four pathologists are presented through (a) - (d). The distribution of the AI algorithm scores is shown in (e). The kappa scores of the AI algorithm and the four pathologists (f) show that the AI algorithm and P_i has the highest agreement, and the AI algorithm, on average pairwise kappa scores, is only second to P_i .

morphology. We validated the performance of the AI algorithm through multiple qualitative and quantitative experiments, and showed that our approach could perform as well as the best performing pathologists. The output of our approach is the full spectrum of tumor pleomorphism, which is easy to analyse, interpret and reproduce. The full pleomorphism spectrum is highlighted for the pathologists to analyse the tumor morphology without having to zoom-in to investigate individual cells in multiple tumor regions. Similarly, overall score of a slide could easily be interpreted by the pathologists from the distribution of the pleomorphism spectrum visualized on the slide. Therefore, our work could be a very efficient tool for pathologists in their daily workflow for nuclear pleomorphism scoring, also leveraging the problem of subjective interpretation due to the deterministic nature of the automated predictions, and therefore improving concordance among pathologists. Our future work will include such a study in which we will investigate whether the addition of the AI algorithm as a support system could improve the agreement between pathologists. Another future work will include the investigation of the prognostic value of the automated scoring of nuclear pleomorphism spectrum in breast histopathology.

4 Methods

ROI-study for the training and validation of the AI algorithm. We collected H&E stained whole slide images of breast cancer resections, denoted as $\mathbb{W} = \{\mathcal{W}_1, \mathcal{W}_2, \dots, \mathcal{W}_S\}$, with a total number of $S = 39$ slides from two cohorts, which we refer to as cohort A and cohort B. The slides in cohort A were scanned on a 3DHitech P1000 scanner at $0.25 \mu\text{m}/\text{pixel}$, and the slides in cohort B were scanned on a 3DHitech Panoramic 250 Flash II scanner at the same spatial resolution of $0.25 \mu\text{m}/\text{pixel}$. From the cohort A; we made a balanced selection of cases with respect to the nuclear pleomorphism scores. Invasive Ductal Carcinoma (IDC) was the most prevalent tumor type, seen in 24 out of the 31 slides, resembling the distribution of breast cancer patients in clinical practice. From the cohort B; we included 8 additional cases that covered different histological subtypes with severely aberrant morphology from a triple negative breast cancer cohort. As a result, pleomorphism of the tumor with score 3 in cohort A was, on average, less severe than the tumor with score 3 in cohort B. Overall, the slides were selected to cover the entire range of nuclear pleomorphism from a large spectrum of tumor morphology in breast cancer pathology, as presented in Table 2.

In routine clinical practice, normal epithelium in a whole slide image, when present, is a useful reference point for pathologists to determine the degree of pleomorphism of the tumor. In the ROI-study, we present pairs of ROIs from tumor and

Invasive carcinoma type	ROI-study		Slide-study
	Slides	ROIs	Slides
Ductal	26	83	90
Lobular	6	21	23
Metaplastic carcinoma	3	8	-
Invasive micropapillary	1	4	2
Mucinous	1	3	-
Tubular	1	3	2
Malignant adenomyoepithelioma	1	3	-
Cribriform	-	-	1
Total	39	125	118

Table 2. Distribution of the tumor types in the ROI and slide studies.

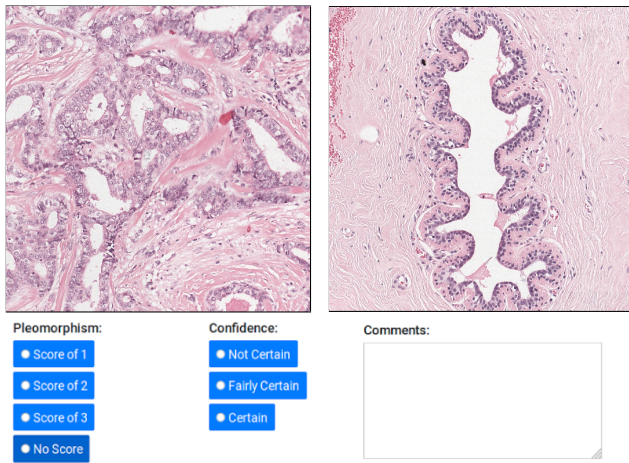
normal epithelium to the pathologists to perform nuclear pleomorphism scoring similar to the routine practice. We manually selected one or more tumor ROIs from each slide, $\hat{\mathcal{R}}_s = \{\hat{R}_{s1}, \hat{R}_{s2}, \dots, \hat{R}_{st_s}\}$, ensuring score homogeneity of tumor cells within each ROI where t_s denotes the number of selected tumor regions from slide \mathcal{W}_s . Overall, we selected $T = 125$ such regions from 39 slides, $\hat{\mathbb{R}} = \{\hat{\mathcal{R}}_1, \hat{\mathcal{R}}_2, \dots, \hat{\mathcal{R}}_T\} \subset \mathbb{W}$. Additionally, we manually selected at least one ROI, $\bar{\mathcal{R}}_s = \{\bar{R}_{s1}, \bar{R}_{s2}, \dots, \bar{R}_{sn_s}\}$ from normal epithelium (normal ROI), where n_s denotes the number of such regions selected from the slide \mathcal{W}_s . As few slides contained little to no large enough areas with normal epithelium, it was not possible to select at least one normal ROI from every slide. In total, there were 59 normal ROIs that we could select from the set of slides, $\bar{\mathbb{R}} = \{\bar{\mathcal{R}}_1, \bar{\mathcal{R}}_2, \dots, \bar{\mathcal{R}}_N\} \subset \mathbb{W}$. Ten out of the 39 slides did not have large enough region with normal cells. Therefore, for the whole slide images without normal epithelium, we retrieved 10 additional slides from the same patient to acquire at least one normal ROI. As a result, the total number of selected normal ROIs increased to $N = 79$ with the selection of additional 20 normal ROIs from the extra set of slides. Following this selection procedure, each ROI was cropped around their center point to a standard square area of around 0.38 mm^2 at $40\times$ magnification. Subsequently, a tumor ROI was paired with a normal ROI from the same patient to form a query pair, $Q_{s,jk} = \{\hat{R}_{sj}, \bar{R}_{sk}\}$, $j = \{1, \dots, t_s\}$, $k \in \{1, \dots, n_s\}$. This process is repeated for all 125 tumor ROIs in this data set. It has to be noted that each query had a unique tumor ROI, but a normal ROI could be paired with more than one tumor ROI due to the smaller number of normal ROIs vs tumor ROIs, 79 vs 125.

We built a web-based nuclear pleomorphism platform consisting of the queries to display the ROIs, allowing the pathologists to score them through a user interface. Each query was followed by the questions; nuclear pleomorphism score of the tumor into one of the three categories; 1, 2 or 3, and an optional field for confidence with the scoring; not certain, fairly certain, certain, as well as an additional text field for comments about the queried tumor and normal ROIs. An example is provided in Figure 7a. In the figure, the ROIs were displayed on a smaller resolution. When an ROI is selected, the full resolution of the ROI was displayed with a total size of 2560×2560 pixels. We invited 10 pathologists from several countries with varying levels of expertise in breast pathology to participate in this study. As a result, each tumor ROI, \hat{R}_t , was scored for nuclear pleomorphism $G = 10$ times, denoted by the set of scores $\{y_t^1, y_t^2, \dots, y_t^G\}$. For a tumor ROI, \hat{R}_t , in the query Q_t , we aggregated the pleomorphism scores of the pathologists by average pooling, referred to as the reference score of \hat{R}_t and is denoted by $y_t^{ref} = \frac{1}{G} \sum_{g=1}^G y_t^g$, $t \in \{1, 2, \dots, T\}$. We present the reference scores as well as the pleomorphism scores of the individual pathologists for the 125 queries in Figure 8. Additionally, we provide the distribution of the scores of the pathologists with respect to the reference scores, categorized by their confidence scores in Figure 9. Throughout our experiments, we train and validate the AI algorithm on a large subset of this data set, using the reference scores as reference standard. The rest of this data set was used to evaluate the ROI-level performance of the AI algorithm compared to the pathologists. A more detailed breakdown of the training, validation and evaluation subsets is provided in the experimental settings section.

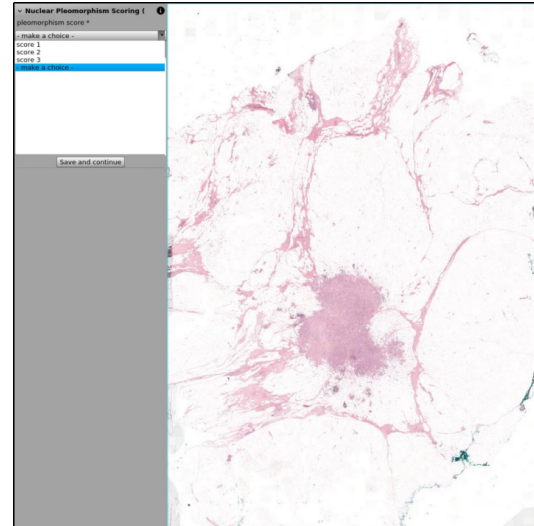
Slide-study for the evaluation of the AI algorithm. We collected an additional set of H&E stained whole slide images from the cohort B, $\mathbb{V} = \{\mathcal{V}_1, \mathcal{V}_2, \dots, \mathcal{V}_Z\}$, with a total number of $Z = 118$ slides. The slides selected for this study did not share any overlap with the ROI-study, as the patients in each study were unique. The selection criteria for the slides followed a similar approach to ROI-study, where we collected a large variety of slides with diverse tumor cell morphology. We used the available clinical data of the patients to approximate the distribution in the clinical practice. IDC was the most prevalent type of cancer with 71 slides, whereas the second most was Invasive Lobular Carcinoma (ILC) with 14 slides. The full distribution of the tumor types in the slide-study is presented in Table 2.

A web platform ¹ was built for scoring nuclear pleomorphism on the 118 slides. The application could display multi-

¹www.grand-challenge.org



(a) An example query from the web platform of the ROI-study with a pair of tumor and normal ROIs from the same patient. Ten pathologists are invited to score nuclear pleomorphism and provide confidence scores for such 125 queries from 39 whole slide images.



(b) An example query from the web platform for the slide-study. Four pathologists are invited to score nuclear pleomorphism for 118 whole slide images.

Figure 7. The web platforms utilized for the (a) ROI-study and (b) slide-study.

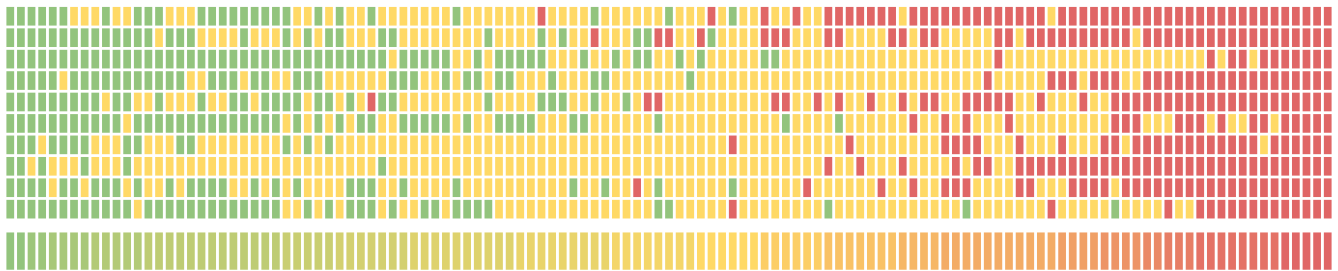


Figure 8. Distribution of the nuclear pleomorphism scores of the pathologists and of the average (reference) scores of the pathologists in the ROI-study. Each row corresponds to a pathologist, except for the last row which corresponds to the average scores of the pathologists which we use as reference scores in our learning setup. Each column is one of the 125 queries in the ROI-study. The colors green, yellow and red correspond to the scores of 1, 2 and 3 of the pathologists, respectively. The queries are sorted by the average scores, from left to right in increasing order, denoted by the color hues of green, yellow and red, corresponding to the increasing severity of the pleomorphism.

resolution whole-slide images to enable the pathologists to freely navigate the slide with zoom-in and zoom-out capabilities. In this slide-level study, we requested from pathologists to score nuclear pleomorphism scores of whole slide images as 1,2 or 3 and provided them an optional comment field for each queried slide, as presented in Figure 7b. We invited three of the 10 pathologists who participated in the ROI-study, to also score nuclear pleomorphism in the slide-study. Moreover, we invited an extra pathologist who did not participate in the ROI-study, bringing the total number of pathologists in this study to four. Detailed breakdown of the score distributions of the pathologists, individually, and compared to each other is displayed in Figure 10. In our experiments, we used the whole slide images and the pleomorphism scores of the pathologists only to evaluate the performance of the AI algorithm, as opposed to the ROI-study where training and validation of the AI algorithm were also carried out.

A two-stage approach for nuclear pleomorphism. We propose a two-stage methodology to score nuclear pleomorphism on whole slide images in breast cancer, following the routine practice in which pathologists analyze the tumor in several cancer zones and compare the morphology of the tumor to the morphology of the cells in normal epithelium. Therefore, the first stage consists of the detection of tumor and normal cells using our epithelial cell detection network. For the second stage, we propose to train a deep regression network to learn nuclear pleomorphism scoring as a spectrum, considering it as a continuum instead of the traditional three-category classification. Additionally, we propose an extension to the deep regression network to

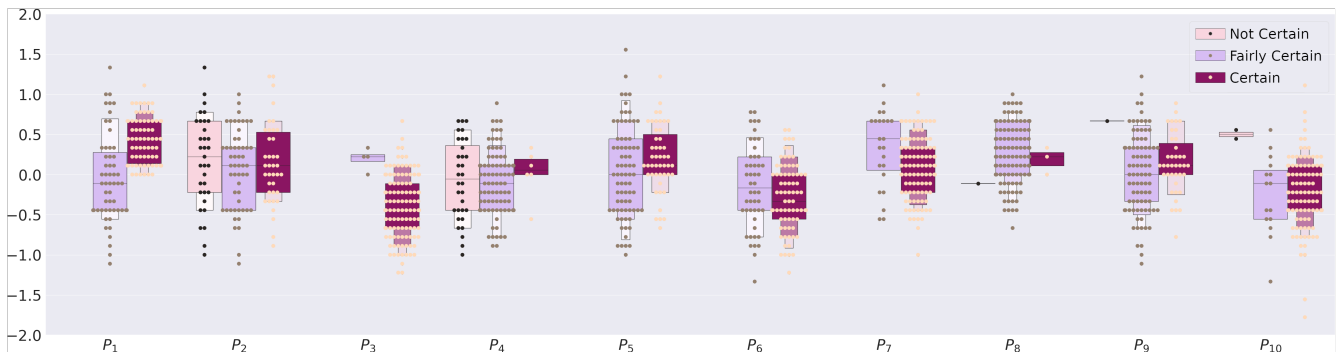


Figure 9. Nuclear pleomorphism score distribution of the pathologists in the ROI-study with respect to their difference from the reference scores, categorized by pathologist confidence. Each box plot and the points within correspond to the score differences of a pathologist from the reference scores, categorized by the confidence of the pathologist; not certain, fairly certain and certain, from left to right. Here, we left the scores of a pathologist out of the computation of the reference scores in order to compare that pathologist to other 9 pathologists.

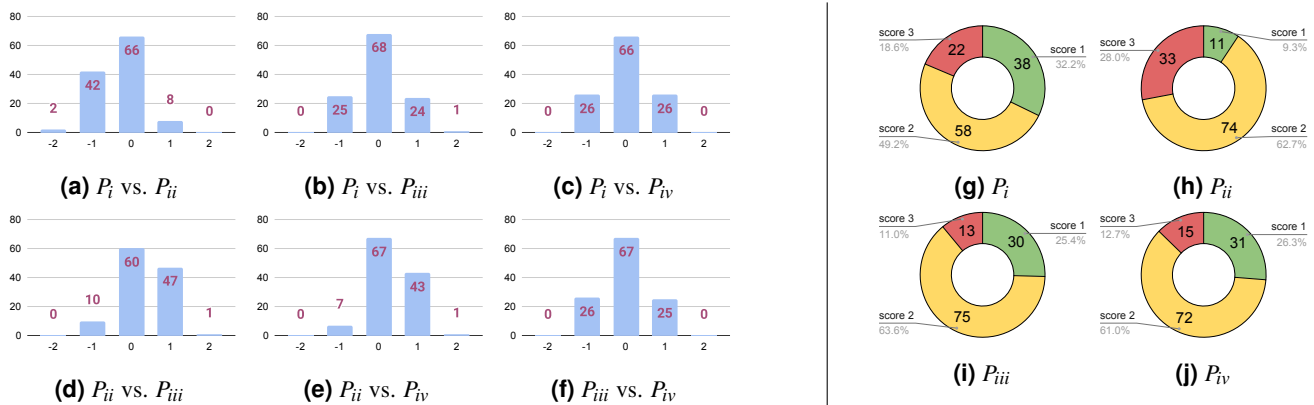


Figure 10. The comparison of the pleomorphism scores of the four pathologists (a)-(f) as well as the score distribution of the pathologists (g)-(j) in the slide-study display the scoring patterns of the pathologists on the 118 whole slide image in the slide-study. The largest differences were observed between P_{ii} and other pathologists, with P_{ii} assigning significantly lower number of score 1s and much higher number of score 3s compared to the other three pathologists.

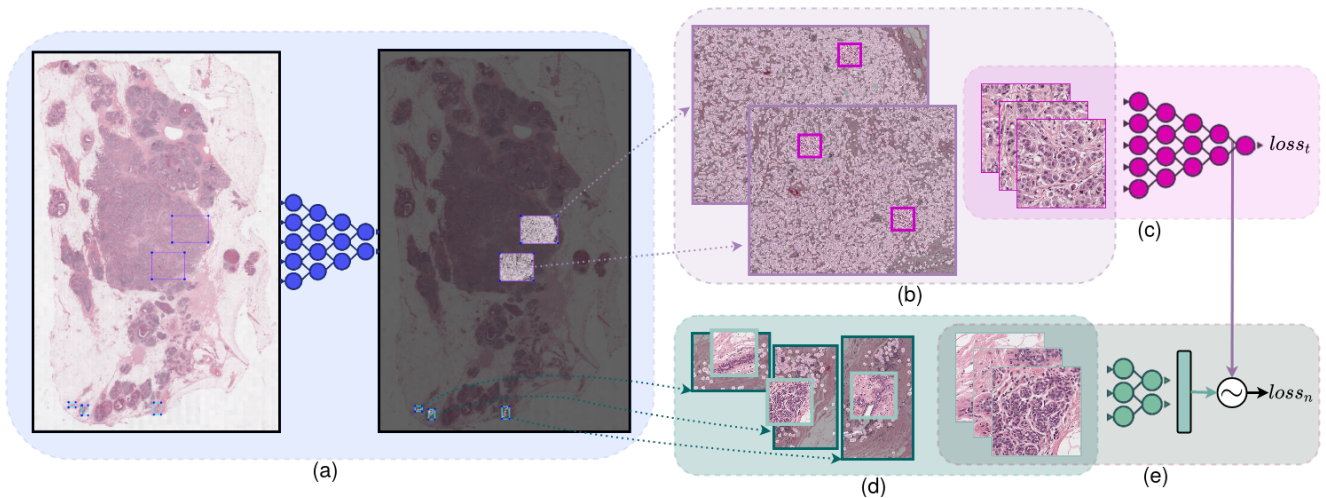


Figure 11. Proposed methodologies for scoring nuclear pleomorphism, (a)-(c) by tumor morphology as a spectrum and (a)-(e) by incorporating additional knowledge from normal epithelium. The weights of the epithelial cell detection network (a) were kept frozen during the training of the deep regression network (c) for regressing pleomorphism spectrum as well as during the joint training using the feature embedding network (e) for the investigation of the added value of normal epithelium as baseline.

discuss the additional benefit of incorporating knowledge from normal epithelium. An illustration of the proposed two-stage methodology as well as the extension to the deep regression network is presented in Figure 11.

Tumor detection and patch sampling by tumor density. In the first stage of our methodology, we use the epithelial cell detection network to find the tumor and normal cells in the ROIs from the whole slide images in the ROI-study. This network is based on one of the state-of-the-art single-shot object detection networks, RetinaNet [21], which we had trained on annotated nuclei for the detection of tumor and normal cells in our previous work. In this work, we use this network to ensure that the patches sampled from the ROIs during the training of the pleomorphism scoring network contains high cellular activity. It is particularly important to ensure tumor density in the sampled patches for the deep regression network to learn to make its predictions based on tumor cells, and not on other factors in the tissue. For inference, the epithelial cell detection network is used to process whole slide images to detect and segment the tumor regions for the deep regression network to score nuclear pleomorphism only in diagnostically relevant regions. Throughout the learning procedure, epithelial cell detection network was only used for inference purposes keeping the network weights frozen.

Nuclear pleomorphism as a continuum. Nuclear pleomorphism is traditionally scored into one of the three categories, 1, 2 or 3, according to the grading criteria. Even though the clinical practice mostly follows this scoring criterion, pathologists can introduce more sensitivity by adding or subtracting half a score when the pleomorphism of the tumor is difficult to categorize. Motivated by this practice in clinic and our observation from the ROI-study (Figure 8), we propose a more generalized version of the categorical classification by considering the nuclear pleomorphism as a continuous spectrum of the change in tumor morphology. This realization transforms the three-category classification problem into a regression task on the full nuclear pleomorphism spectrum. The granularity in the pleomorphism spectrum was made possible by the averaged collective knowledge of the 10 pathologists. Therefore, the second stage in our methodology is comprised of a deep regression network based on Densenet [16], which is trained on patches sampled by tumor density from the ROIs using the average (reference) scores of the pathologists as reference standard. A Densenet architecture consists of the so-called 'dense blocks' in which the input $x^{(l)}$ of a layer l is the concatenation of the output of the previous block and the inputs of the layers preceding it, $x^{(l)} = [x, f^1(x), f^2([f^1(x), x]), \dots, f^l([f^{l-1}([\dots, x]), x])]$. Another distinguishing feature of Densenet was the addition of the so-called 'transition layers', which help to regulate the number of channels in the network. In comparison, a traditional CNN is only composed of consecutive layers, in which an input of a layer is the output of the previous layer, $x^{(l)} = f^{l-1}(f^{l-2}(\dots(x)))$. A training iteration of our Densenet based deep regression network is as follows. A training patch \hat{x}_t^i , sampled from the tumor ROI, \hat{R}_t , is fed through the deep regression network to regress its pleomorphism score $f(\hat{x}_t^i) \in [1 - \epsilon, 3 + \epsilon]$. The smoothL1

Layer	Feature embedding network
1	conv(7,3,0)-32 + maxpool(2,2) + ReLU + BN
2	conv(5,2,0)-64 + maxpool(2,2) + ReLU + BN
3	conv(3,3,0)-64 + maxpool(2,2) + ReLU + BN
4	conv(3,3,0)-128 + maxpool(2,2) + ReLU + BN
5	fc(512,256) + ReLU
6	fc(256,1024) + ReLU

Table 3. The deep regression network was extended by the feature embedding network to investigate the added value that can be learned from normal epithelium. conv(k, s, p)- c_o is a convolutional layer with kernel size k , stride of s , padding of p , with c_o number of output channels, maxpool(k, k) is the max pooling operation with kernel size of k , ReLU corresponds to rectified linear unit, and BN refers to batch normalization. fc(c_i, c_o) is a fully connected layer with c_i number of input and c_o number of output channels.

loss function is computed from the predicted value $f(\hat{x}_t^i)$ with respect to the reference score $y_t^{ref} \in [1, 3]$ as

$$loss_t = smooth_{L1}(f(\hat{x}_t^i) - y_t^{ref}),$$

$$smooth_{L1}(x) = \begin{cases} |x| & \text{if } |x| > \alpha, \\ \frac{1}{\alpha}x^2 & \text{if } |x| \leq \alpha \end{cases}$$

where α is the hyperparameter of the loss function, corresponding to the degree of the contribution of L_1 and L_2 losses, which we set to the default value of 1 in our experiments. Finally, the gradient of the loss function is backpropagated through the network to improve the prediction performance in the next iteration by updating the network weights. This training iteration is done on a batch of multiple such patches from various tumor ROIs in the training set, $\hat{\mathbf{x}} = \{\hat{x}^1, \hat{x}^2, \dots, \hat{x}^B\}$, with B denoting the batch size. This process of one iteration in training is visualized in Figure 11 through (a) to (c). Tens of thousands of patches sampled from the tumor ROIs in the training set as well as the granularity of the reference nuclear pleomorphism scores make it possible for the network to analyse a diverse tumor morphology as a spectrum.

Added value of normal epithelium as baseline. Following the routine clinical workflow in which normal epithelium is used as baseline for the nuclear pleomorphism scoring of tumor, we propose an extension to our deep regression network in order to investigate the additional value that can be leveraged from the morphology of normal cells. In this extended deep regression network, the tumor patches, $\hat{\mathbf{x}} = \{\hat{x}^1, \hat{x}^2, \dots, \hat{x}^P\}$, are used as input to the Densenet architecture, as before. The normal patches, $\bar{\mathbf{x}} = \{\bar{x}^1, \bar{x}^2, \dots, \bar{x}^P\}$, are fed through a simpler feature embedding network, denoted by g , as normal cells have little to no variability in morphology compared to the large plethora of the tumor morphology. The architectural details of the feature embedding network are outlined in Table 3. In this extension, the feature representation from a tumor patch is compared to the feature embedding from a normal patch through a cosine similarity loss function

$$loss_n = \max\left(0, \left[\phi(y_t^{ref}) \cos(f^p(\hat{x}_t^i), g(\bar{x}_n^j))\right]\right),$$

$$\phi(y_t^{ref}) = 0.5y_t^{ref} - 1$$

where $y_t^{ref} \in [1, 3]$ is the reference score of the tumor patch \hat{x}_t , f^p denotes the penultimate layer of the deep regression network from which the feature representation of the tumor patch is obtained. This loss function ensures that the feature representations of the tumor patches with reference scores around 1 will resemble the most to the normal patches, and the patches with reference scores closer to 3 will resemble the least. More specifically, the feature representation of a tumor patch with size 1024 from the penultimate layer of the deep regression network is compared to the output of a normal patch with the same size from the feature embedding network. The cosine similarity function is parameterized by a function of the reference score of the tumor patch to control the penalization with respect to the similarity versus the normal patch. During learning, both the deep regression network and the feature embedding network are trained jointly, utilizing both loss functions $loss_t$ and $loss_n$. During inference, only the deep regression network is used to predict a pleomorphism score for an input image patch. Similar to the first approach, the epithelial cell detection network is employed to ensure high cellular density in sampled tumor and normal patches. The rest of the training procedure such as the selection of hyperparameters were kept the same as before. This extended deep regression network is visualized in Figure 11 through (a) to (e).

Experimental Setting. The majority of the data set collected in the ROI-study was mainly used for the training and the validation of the AI algorithm, and only a small subset was used for evaluation. On the other hand, the entire set of the whole

slide images in the slide-study were only used for evaluation. The selection of the slides for the training and the validation of the AI algorithm was carried out with the goal of exposing it to as much variety of tumor morphology as possible. As a result, we selected the 52 ROIs from 16 slides and the 28 ROIs from 10 slides in the ROI-study. The remaining 45 ROIs from the 13 slides were used to evaluate the performance of the AI algorithm. The performance evaluation in the ROI-study could be regarded as the result of a controlled experiment in which each test ROI was homogeneous in nuclear pleomorphism severity. The 118 slides from the slide-study were only used for slide-level performance evaluation of the AI algorithm compared to the pathologists. This setting represented the real-world clinical practice where the AI algorithm scored nuclear pleomorphism on whole slide images.

We trained the Densenet based deep regression network from scratch using the Adam optimizer with a learning rate of $1e-4$. Each training patch was 512×512 pixels, extracted from the tumor ROIs in the training set of the ROI-study slides at 0.5 spacing. The batch size used during an iteration of the training was 12. Each epoch contained 200 training and 500 validation iterations. Training of the deep regression network continued until the loss value in the validation set no longer improved. The training and validation patches were augmented with spatial operations such as horizontal and vertical flips and 90° , 180° , 270° rotations. In order to make the AI algorithm color and stain invariant, we applied heavy color and stain augmentations on the training patches [36]. The training patches were also augmented with blurring techniques to make the network more robust against out-of-focus artifacts, commonly seen in whole slide images. A Gaussian map was applied on the output of the epithelial cell detection network to create a density map of the tumor cells which was used to sample patches from areas with high cellular density during training. A batch had a balanced pleomorphism distribution among its patches, which was made possible by an equal distribution of quantized reference scores.

The performance of the deep regression network was compared to the performance of the extended deep regression network to investigate the added value of normal epithelium as a baseline, using several regression metrics, such as mean absolute error (*MAE*), mean squared error (*MSE*) and median absolute error (*MdAE*), explained variance score (*EV*) and R^2 score. Throughout the other quantitative evaluations, the predictions of the AI algorithm were quantized into several categories, most notably into the traditional three-category setting to compare the performance against the pathologists. To illustrate, quantization of the range $[1, 3]$ into three categories was to partition the score spectrum into three equal sized categories; a prediction within the range of $[1, 1.66)$ corresponded to score 1, $[1.66, 2.33]$ corresponded to score 2, and $(2.33, 3]$ corresponded to score 3. We evaluated the performance of the AI algorithm versus the pathologists as well as the performance of each pathologist versus one another, by Cohen’s quadratic kappa measure [25]

$$\kappa = \frac{p_o - p_e}{1 - p_e}$$

where p_o denotes the relative observed agreement between two participants and p_e corresponds to the probability of chance agreement.

5 Acknowledgements

This research has been supported by the NWO-Perspectief program EDL (Efficient Deep Learning), co-financed by the Dutch Organisation for Scientific Research and 35 Dutch companies.

References

- [1] Janowczyk A and Madabhushi A. “Deep Learning for Digital Pathology Image Analysis: A Comprehensive Tutorial with Selected Use Cases”. In: *Journal of Pathology Informatics* 7.29 (July 2016).
- [2] Balázs Ács, Mattias Rantalainen, and Johan Hartman. “Artificial Intelligence as the Next Step Towards Precision Pathology”. In: *Journal of Internal Medicine* 288.1 (July 2020), pp. 62–81.
- [3] Maschenka C. A. Balkenhol et al. “Deep Learning and Manual Assessment Show That the Absolute Mitotic Count Does Not Contain Prognostic Information in Triple Negative Breast Cancer”. In: *Cellular Oncology* 42.4 (Aug. 2019), pp. 555–569.
- [4] Maschenka C. A. Balkenhol et al. “Deep Learning Assisted Mitotic Counting for Breast Cancer”. In: *Laboratory Investigation* 99.11 (June 2019), pp. 1596–1606.
- [5] Babak Ehteshami Bejnordi et al. “Diagnostic Assessment of Deep Learning Algorithms for Detection of Lymph Node Metastases in Women with Breast Cancer”. In: *JAMA* 318.22 (2017), pp. 2199–2210.
- [6] Kaustav Bera et al. “Artificial Intelligence in Digital Pathology—new Tools for Diagnosis and Precision Oncology”. In: *Nature Reviews Clinical Oncology* 16.11 (Aug. 2019), pp. 703–715.

- [7] H. Bloom and W. Richardson. “Histological Grading and Prognosis in Breast Cancer”. In: *British Journal of Cancer* 11.3 (1957), pp. 359–377.
- [8] Wouter Bulten et al. “Artificial Intelligence Assistance Significantly Improves Gleason Grading of Prostate Biopsies by Pathologists”. In: *Modern Pathology* (Aug. 2020).
- [9] Wouter Bulten et al. “Automated Deep-learning System for Gleason Grading of Prostate Cancer using Biopsies: A Diagnostic Study”. In: *Lancet Oncology* 21 (2 Feb. 2020), pp. 233–241.
- [10] Dan C. Cireşan et al. “Mitosis detection in breast cancer histology images with deep neural networks”. In: *Medical Image Computing and Computer-Assisted Intervention*. 2013.
- [11] Jacob Devlin et al. “Bert: Pre-training of Deep Bidirectional Transformers for Language Understanding”. In: *North American Chapter of the Association for Computational Linguistics*. 2018.
- [12] C. Elston and Ian Ellis. “Pathological Prognostic Factors in Breast Cancer. I. The Value of Histological Grade in Breast Cancer: Experience from a Large Study with Long-term Follow-up”. In: *Histopathology* 19.5 (Nov. 1991), pp. 403–410.
- [13] Henry F. Frierson Jr. et al. “Interobserver Reproducibility of the Nottingham Modification of the Bloom and Richardson Histologic Grading Scheme for Infiltrating Ductal Carcinoma”. In: *American Journal of Clinical Pathology* 103.2 (Feb. 1995), pp. 195–198.
- [14] Ziba Gandomkar, Patrick C. Brennan, and Claudia Mello-Thoms. “Computer-Assisted Nuclear Atypia Scoring of Breast Cancer: a Preliminary Study”. In: *Journal of digital imaging* 32.5 (Oct. 2019), pp. 702–712.
- [15] Paula S. Ginter et al. “Histologic Grading of Breast Carcinoma: A Multi-institution Study of Interobserver Variation using Virtual Microscopy”. In: *Modern Pathology* (2020), pp. 1–9.
- [16] Gao Huang et al. “Densely Connected Convolutional Networks”. In: *Computer Vision and Pattern Recognition*. 2017.
- [17] Adnan Mujahid Khan, Korsuk Sirinukunwattana, and Nasir Rajpoot. “A Global Covariance Descriptor for Nuclear Atypia Scoring in Breast Histopathology Images”. In: *IEEE journal of biomedical and health informatics* 19.5 (June 2015), pp. 1637–1647.
- [18] A. Krizhevsky, I. Sutskever, and G. Hinton. “Imagenet Classification with Deep Convolutional Neural Networks”. In: *Advances in Neural Information Processing Systems*. 2012.
- [19] Quoc Le et al. “Building High-level Features using Large Scale Unsupervised Learning”. In: *International Conference in Machine Learning*. 2013.
- [20] Soonam Lee et al. “Automatic Glandular and Tubule Region Segmentation in Histological Grading Of Breast Cancer”. In: *Electronic Imaging* 2018.15 (Jan. 2018), pp. 199–1.
- [21] Tsung-Yi Lin et al. “Focal Loss for Dense Object Detection”. In: *International Conference on Computer Vision*. 2017.
- [22] Teri A. Longacre et al. “Interobserver Agreement and Reproducibility in Classification of Invasive Breast Carcinoma: An Nci Breast Cancer Family Registry Study”. In: *Modern Pathology* 19.2 (Feb. 2006), pp. 195–207.
- [23] Cheng Lu et al. “Automated Image Analysis of Nuclear Atypia in High-power Field Histopathological Image”. In: *Journal of Microscopy* 258.3 (June 2015), pp. 233–240.
- [24] P. Maqlin et al. “Automated Nuclear Pleomorphism Scoring in Breast Cancer Histopathology Images Using Deep Neural Networks”. In: *International Conference on Mining Intelligence and Knowledge Exploration*. 2015.
- [25] Mary L. McHugh. “Interrater Reliability: The Kappa Statistic”. In: *Biochemia medica* 22.3 (Oct. 2012), pp. 276–282.
- [26] Caner Mercan et al. “From Point Annotations to Epithelial Cell Detection in Breast Cancer Histopathology using RetinaNet”. In: *Medical Imaging with Deep Learning*. 2019.
- [27] John S. Meyer et al. “Breast Carcinoma Malignancy Grading by Bloom–richardson System vs. Proliferation Index: Reproducibility of Grade and Advantages of Proliferation Index”. In: *Modern Pathology* 18.8 (Aug. 2005), pp. 1067–1078.
- [28] Kunal Nagpal et al. “Development and Validation of a Deep Learning Algorithm for Improving Gleason Scoring of Prostate Cancer”. In: *NPJ digital medicine* 2.1 (2019), pp. 1–10.
- [29] Kien Nguyen et al. “Tubule Segmentation of Fluorescence Microscopy Images Based on Convolutional Neural Networks with Inhomogeneity Correction”. In: *Proceedings of the SPIE*. 2015.
- [30] Muhammad K. K. Niazi, Anil V. Parwani, and Metin N. Gurcan. “Digital Pathology and Artificial Intelligence”. In: *Lancet Oncology* 20.5 (May 2019), e253–e261.

- [31] Henri Noël et al. “Detection of High-grade Atypia Nuclei in Breast Cancer Imaging”. In: *Proceedings of the SPIE*. 2015.
- [32] David Romo-Bucheli et al. “Automated Tubule Nuclei Quantification and Correlation with Oncotype Dx Risk Categories in Er+ Breast Cancer Whole Slide Images”. In: *Nature Scientific Reports* 6 (Sept. 2016), p. 32706.
- [33] Ramprasaath R. Selvaraju et al. “Grad-cam: Visual Explanations from Deep Networks via Gradient-based Localization”. In: *International Conference on Computer Vision*. 2017.
- [34] Rebecca L. Siegel, Kimberly D. Miller, and Ahmedin Jemal. “Cancer Statistics, 2020”. In: *CA: A Cancer Journal for Clinicians* 70.1 (2020), pp. 7–30.
- [35] David Silver et al. “Mastering the Game of Go with Deep Neural Networks and Tree Search”. In: *Nature* 529.7587 (2016), pp. 484–489.
- [36] David Tellez et al. “Quantifying the Effects of Data Augmentation and Stain Color Normalization in Convolutional Neural Networks for Computational Pathology”. In: *Medical image analysis* 58 (Dec. 2019), p. 101544.
- [37] David Tellez et al. “Whole-Slide Mitosis Detection in H&E Breast Histology Using PHH3 as a Reference to Train Distilled Stain-Invariant Convolutional Networks”. In: *IEEE Transactions on Medical Imaging* 37.9 (Sept. 2018), pp. 2126–2136.
- [38] Mitko Veta et al. “Assessment of Algorithms for Mitosis Detection in Breast Cancer Histopathology Images”. In: *Medical Image Analysis* 20.1 (Feb. 2015), pp. 237–248.
- [39] Mitko Veta et al. “Predicting Breast Tumor Proliferation from Whole-slide Images: the TUPAC16 Challenge”. In: *Medical Image Analysis* 54.5 (May 2019), pp. 111–121.